



Contents lists available at ScienceDirect

Spectrochimica Acta Part A: Molecular and Biomolecular Spectroscopy

journal homepage: www.elsevier.com/locate/saa

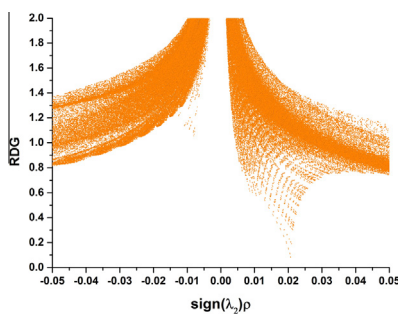
The spectroscopic and quantum chemical studies of 3,4-difluoroaniline

Etem Kose^a, Mehmet Karabacak^b, Ahmet Atac^{a,*}^a Department of Physics, Celal Bayar University, Manisa, Turkey^b Department of Mechatronics Engineering, H.F.T. Technology Faculty, Celal Bayar University, Turgutlu, Manisa, Turkey

HIGHLIGHTS

- The compound was characterized by FT-IR, FT-Raman, NMR and UV spectroscopy.
- The vibrational frequencies, chemical shifts and electronic absorption wavelengths were calculated by DFT.
- Density of state (TDOS, PDOS, and OPDOS) diagrams for 3,4-difluoroaniline were analyzed.
- Nonlinear optical properties and thermodynamical analysis were investigated.

GRAPHICAL ABSTRACT



ARTICLE INFO

Article history:

Received 28 August 2014

Received in revised form 15 January 2015

Accepted 29 January 2015

Available online 9 February 2015

Keywords:

DFT

3,4-difluoroaniline

FT-IR and FT-Raman

NMR and UV spectra

Density of states

ABSTRACT

Spectroscopic and structural investigations of 3,4-difluoroaniline molecule are presented by using experimental (FT-IR, FT-Raman, ¹H and ¹³C NMR, and UV-Vis) techniques and theoretical (DFT approach) calculations. FT-IR and FT-Raman spectra of 3,4-difluoroaniline molecule are recorded in the region 4000–400 cm⁻¹ and 3500–10 cm⁻¹ in the liquid phase, respectively. The NMR chemical shifts (¹H and ¹³C) are recorded in chloroform-d solution. The UV absorption spectra of 3,4-difluoroaniline dissolved in ethanol and water are recorded in the range of 200–400 nm. Experimental results are supported with the following theoretical calculations; the optimized geometry and vibrational (FT-IR and FT-Raman) spectra are carried out by DFT (B3LYP)/6-311++G(d,p) basis set calculations. The nuclear magnetic resonance spectra (¹H and ¹³C NMR) are obtained by using the gauge-invariant atomic orbital method. Moreover, electronic characteristics, such as HOMO and LUMO energies, density of state diagrams, and molecular electrostatic potential surface are investigated. Nonlinear optical properties and thermodynamic features are also outlined theoretically. An excellent correlation of theoretical and experimental results provides a detailed description of the structural and physicochemical properties of the molecule. Thus, this work leads to a deep understanding of the characteristics of di-substituted aniline derivatives.

© 2015 Elsevier B.V. All rights reserved.

Introduction

Aniline and its substituted derivatives have been used in various industrial and commercial applications, including dyestuff, pesticide, and pharmaceutical manufacturing [1]. The substances and their halogenated derivatives are considered to be environmentally

toxic pollutants releasing into soil and water as wastes of industrial synthesis of many pesticides and plastics, and products of microbial transformation of urea herbicides [2–4]. Moreover, fluoroanilines are especially important due to their interesting biological activities like being key intermediates in the manufacture of agrochemicals (pesticides, herbicides, and fungicides) [5], and serving as precursors in the production of several drugs, such as analgesics, central nervous depressants, and antibiotics [6,7]. Recently, an interesting usage fluoroaniline polymers as precursors in the synthesis of

* Corresponding author. Tel.: +90 236 2013105.

E-mail address: atacahmet2007@gmail.com (A. Atac).

glucose biosensors [8] and modifiers of electrodes in bacterial fuel cells [9] has been reported.

Aniline and its derivatives have been studied extensively by spectroscopic and theoretical methods due to their interesting features and chemical importance. Vibrational assignment based FT-IR in the vapor, solution, and liquid phases and Raman spectrum in the liquid state have already reported for aniline [10]. The structure of aniline was studied experimentally in the gas phase by microwave spectroscopy [11,12] and electron diffraction [13] and in the solid state by X-ray crystallography [14]. Structural analysis of aniline was also reported theoretically by using semi-empirical [15,16] and ab initio methods [15,17,18]. A complete interpretation of the vibrational spectrum of aniline was carried out on the basis of normal coordinate analysis [19]. An exhaustive study of the structural as well as the electronic properties of aniline was obtained using several DFT-based methods [20]. The structures of aniline in the ground and first excited singlet states were calculated by using ab-initio quantum chemical methods [21]. Another detailed structural investigation of aniline in ground and transition states for internal rotation and inversion of the amino group was carried out using several quantum computational methods [22].

Structural and spectroscopic features of some substituted anilines have also been explored in experiments and via theoretical methods. A summary of the studies on some fluorinated derivatives of aniline, in our interest, are gathered as follows: the scaled quantum mechanical force field calculations at the HF/6-31+G(d) level of theory and vibrational Raman spectrum of para-fluoroaniline [23] and far infrared gas spectra of aniline and 4-fluoroaniline (4-FA) are reported [24]. The far-infrared vapor phase spectra of aniline-ND₂ and aniline-NHD were presented [25]. Infrared spectra of fluorinated anilines were performed with some tentative assignments [26,27]. Honda et al. [28] determined the N–H stretching frequencies of aniline, 2-, 3-, and 4-fluoroaniline in the gas phase by using the IR-UV double resonance spectroscopy. Infrared spectrum of 2,3-fluoroaniline were recorded and vibrational assignments for the observed fundamental frequencies were proposed [29]. Recently, Mukherjee and coworkers [30,31] reported vibrational spectra and computational studies of tri-fluoroanilines (2,3,4-, 2,3,6- and 2,4,5-, 2,4,6-) by using HF and B3LYP methods. 3,5-DFA was investigated with experimental and computational methods by Pathak et al. [32]. Theoretical Raman and infrared spectra of para-halogen anilines were obtained and corresponding vibrational assignments were given [33]. Govindarajan et al. [34] investigated spectroscopic analysis of organic 2,4,5-trichloroaniline.

Although several spectroscopic and structural studies have been reported on substituted anilines, as summarized, no report on detailed neither theoretical nor experimental spectroscopic study on the conformational, vibrational, magnetic, and electronic properties of 3,4-difluoroaniline (3,4-DFA). Here, a fully detailed description of 3,4-DFA was carried out theoretically by DFT (B3LYP)/6-311++G(d,p) basis set calculations as well as experimental techniques of FT-IR, FT-Raman, ¹³C and ¹H NMR, and UV-Vis spectra. In addition, temperature dependences of the heat capacity, entropy, and enthalpy of 3,4-DFA molecule were analyzed. The nonlinear optical properties (the dipole moment, anisotropy of polarizability and first hyperpolarizability) of 3,4-DFA molecule were also explored theoretically.

Experimental

3,4-difluoroaniline (C₆H₅NF₂) sample was provided from Across Organics Company in liquid phase with a stated purity of greater than 97% and no further purification. The experimental FT-IR and FT-Raman spectra of the title molecule was recorded in the region 4000–400 cm⁻¹ and 3500–10 cm⁻¹, respectively. Perkin-Elmer FT-

IR System Spectrum BX spectrometer at room temperature, with a scanning speed of 10 cm⁻¹ min⁻¹ and the spectral resolution of 4.0 cm⁻¹ used for FT-IR and Bruker RFS 100/S FT-Raman instrument using 1064 nm excitation from an Nd:YAG laser was used, the detector is a liquid nitrogen cooled Ge detector, five hundred scans were accumulated at 4 cm⁻¹ resolution using a laser power of 100 mW for FT-Raman spectrum. The nuclear magnetic resonance (NMR) (¹H and ¹³C) spectra of 3,4-DFA molecule were carried out in Varian Infinity Plus spectrometer at 300 K. The molecule was dissolved in chloroform-d solution (CDCl₃). The chemical shifts were reported in ppm relative to tetramethylsilane (TMS). Last one UV-Vis spectra of the title molecule were registered in the range of 200–400 nm by using Shimadzu UV-2101 PC, UV-Vis recording Spectrometer, solved in ethanol and water.

Quantum chemical calculations

The DFT with the Becke's three-parameter hybrid functional (B3) [35,36] for the exchange part and the Lee–Yang–Parr (LYP) correlation function [37], accepted as a cost-effective approach has been used to compute optimized structural geometrical parameters, vibrational frequencies (FT-IR and FT-Raman), UV-Vis and (¹H and ¹³C) NMR spectra of the heading molecule. For all calculations were performed tandem with Gaussian 09 suite of quantum chemical codes [38].

The structural parameters after optimized were employed calculations of the vibrational frequencies, isotropic chemical shifts and electronic properties by using B3LYP with 6-311++G(d,p) basis set. However the frequencies were not used directly, the scaling factors were operated as 0.983 up to 1700 cm⁻¹ and 0.958 for greater than 1700 cm⁻¹ [39,40] due to offset the systematic errors caused by basis set incompleteness, neglect of electron correlation and vibrational anharmonicity [41]. Also, to see the most stable structure of 3,4-DFA molecule, the selected torsion angle (for NH₂ group of position) was changed every 10° and molecular energy profile was calculated from 0° to 180°.

The vibrational assignments of fundamental modes were made on accordance of PEDs. The PEDs were calculated from quantum chemically based on vibrational frequencies using VEDA program [42]. Also to get visual animation and for the verification of the normal modes assignment GaussView Program [43] were fallen back on.

The ¹H and ¹³C NMR isotropic chemical shieldings were obtained by using the gauge-invariant atomic orbital (GIAO) method [44,45] as referred optimized parameters with the B3LYP/6-311++G(d,p) method. On the account of the GIAO method is one of the most prevalent approaches for calculating nuclear magnetic shielding tensors and needful for reliable studies of magnetic properties.

To have UV-Vis spectrum, electronic transitions, vertical excitation energies, absorbance and oscillator strengths of 3,4-DFA molecule, the time-dependent DFT (TD-DFT) method was performed. The frontier molecular orbitals (such as HOMO and LUMO) energies were determined also by TD-DFT approach.

The total density of states (TDOS or DOS), the partial density of states (PDOS) and overlap population density of states (OPDOS) spectra were fulfilled using GaussSum 2.2 program [46] by convoluting the molecular orbital information with Gaussian curves of unit height and a FWHM (Full Width at Half Maximum) of 0.3 eV.

The Molecular electrostatic potential surface (MEPs) of 3,4-DFA molecule is depicted and appreciated with the 2D and 3D size. For different temperature (from 100 to 700 K), the thermodynamic properties of the title molecule such that heat capacity, entropy, and enthalpy changes were effectuated. The dipole moment, mean polarizability and first static hyperpolarizability (in other words nonlinear optical (NLO) properties) of 3,4-DFA molecule were

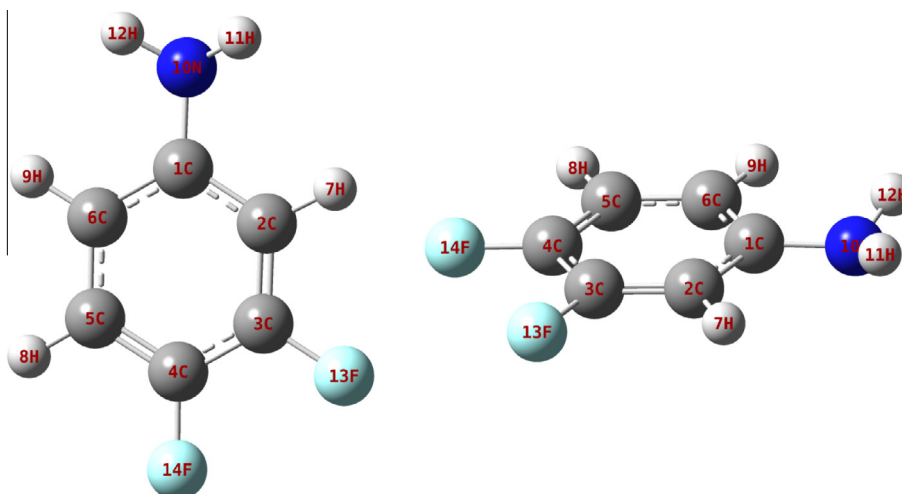


Fig. 1. The theoretical optimized geometric structures of 3,4-DFA.

computed. The reduced density gradient (RDG) of the title molecule were given in graph.

Results and discussion

3,4-DFA molecule has three substituents first one NH_2 group, (had hydrogen atoms attached to nitrogen atom) and two F (fluorine) atoms are at *meta*- and *para* position. We calculated imaginary frequency corresponding to NH_2 wagging for the title molecule in the C_s symmetry point group (410.36 cm^{-1}). The calculations showed that the molecule is unstable in C_s symmetry due to this imaginary frequency. However, the present molecule has positive frequencies in the C_1 point group symmetry. Therefore, in this study, the calculations were done according to the C_1 point group symmetry.

Potential energy surface (PES) scan and energetics

To explain conformational features of the title molecule, a conformation analysis was done between aniline ring and NH_2 group. To analysis conformational flexibility of 3,4-DFA, as a function of $T(\text{H}_{12}-\text{N}_{10}-\text{C}_1-\text{C}_2)$, torsion angle was varied from 0° to 180° by changing every 10° by using B3LYP/6-311++G(d,p) method. The potential energy curve was performed by using scanning NH_2 group made over the phenyl ring. The conformational analysis of the molecule showed that there are one local minimum near 20° (or 160°) torsion angle, given in Fig. S1. It is clear that the molecule was more stable for ca. 20° (or ca. 160°) torsion angle. The discussion below the geometric parameters, vibrational frequencies, NMR shifts and UV-Vis absorption spectrum of the present molecule (C_1 point group symmetry) were reported by using 6-311++G(d,p) basis set with the comparing experimental results.

Geometrical structures

The crystallography data of the present molecule has not been determined yet, because of this the optimized structural parameters of 3,4-DFA molecule calculated at density functional B3LYP method with 6-311++G(d,p) basis sets are being compared with experimentally available X-ray data for aniline [14]. The optimized structure of 3,4-DFA molecule was schemed in Fig. 1 with the atomic numbers. Also the parameters of the optimized structure (bond lengths and angles) of the molecule are given in Table 1

accordance number of Fig. 1. There are seen some discrepancies of the molecular geometry between the theoretical results and experimental results [14]. This can be due to the theoretical results belong to vapor phase and the experimental results belong to liquid phase and also had aniline molecule.

The calculated values of C–C bond lengths are showed very good agreement with the experimental results of aniline (see Table 1). The observed differences can be the effects of F atoms. The calculated bond lengths of C–C in the range from 1.384 to 1.403 Å for B3LYP with 6-311++G(d,p) basis set which are in good agreement with 1.367–1.404 Å and 1.364–1.407 Å for aniline [14]. The result of C–C bond lengths was showed very good correlation in the literature for the structurally similar molecules [30–33,40,47,48].

The optimized value of C_1-N_{10} (NH_2) bond length distance of ca. 1.397 Å is just 0.01 Å lower and 0.11 Å bigger than the reported experimental values of 1.398 and 1.386 Å for aniline [14]. Also the C– NH_2 bond lengths were calculated at 1.389 and 1.388 Å for 2,4,5-TFA and 2,4,6-TFA, respectively [31]. The optimized NH_2 (amino group) bond length is computed at 1.009 Å by B3LYP. Some small differences can be saying by comparing this value with experimental values of 1.070 and 0.940 Å and 0.990 and 0.770 Å. The fluorine atom in the *para*-position of aniline causes a slight elongation of C–N and N–H bonds, a decrease of the HNH angle, and the enlargement of the angle between NH_2 plane and the ring plane, in comparison to aniline [33]. The similar causes and results are seen in this paper see in Table 1. The N–H bond lengths are computed nearly equal as compared to the initial values for aniline [14], which infers that the N–H bonds are not sensitive regarding to the presence of F atom (s) in the ring. The same results were presented in the literature [31,33].

The substitution on aniline ring has been found to change this angle and also affects the degree of pyramidalisation by resonance effects than inductive effects [49,50]. The nitrogen is pyramidal, with the dihedral angle between the plane of the aromatic ring and NH_2 plane being 37.5° [51]. This dihedral angle between NH_2 plane and the plane of the aromatic ring was found as 33.3° [52]. In this study the dihedral angles are computed at -25.1° and 23.6° showing good correlation above related molecules [49–52].

The substitution with F atoms at C_3 , C_4 atoms and also NH_2 group at C_1 leads to some changes of the bond lengths and angles in the aromatic ring. For example $\text{C}_2-\text{C}_1-\text{C}_6$, $\text{C}_2-\text{C}_3-\text{C}_4$, $\text{C}_3-\text{C}_4-\text{C}_5$ ring CCC angles and $\text{C}_1-\text{C}_6-\text{H}_9$, $\text{C}_5-\text{C}_6-\text{H}_9$, $\text{C}_2-\text{C}_3-\text{H}_7$ and $\text{C}_6-\text{C}_5-\text{H}_8$ bonds angles deviated from the negative and positive from the

Table 1
Bond lengths (Å) and bond angles (°) experimental aniline molecule and the optimized of 3,4-DFA molecule.

Parameters	Aniline X-ray[14]	B3LYP	
<i>Bond lengths (Å)</i>			
C ₁ –C ₂	1.404 (6)	1.407 (6)	1.403
C ₁ –C ₆	1.386 (6)	1.385 (6)	1.403
C ₁ –N ₁₀	1.398 (6)	1.386 (6)	1.397
C ₂ –C ₃	1.380 (7)	1.389 (7)	1.384
C ₂ –H ₇	1.030 (3)	1.060 (5)	1.084
C ₃ –C ₄	1.386 (7)	1.364 (7)	1.389
C ₃ –X ₁₃ ^a	1.050 (5)	0.920 (4)	1.348
C ₄ –C ₅	1.391 (7)	1.383 (7)	1.384
C ₄ –X ₁₄ ^a	1.050 (5)	0.970 (7)	1.352
C ₅ –C ₆	1.367 (7)	1.379 (7)	1.392
C ₅ –H ₈	1.050 (5)	0.920 (5)	1.083
C ₆ –H ₉	0.870 (5)	0.890 (5)	1.084
N ₁₀ –H ₁₁	1.070 (5)	0.990 (4)	1.009
N ₁₀ –H ₁₂	0.940 (6)	0.770 (6)	1.009
<i>Bond angles (°)</i>			
C ₂ –C ₁ –C ₆	117.9 (4)	117.9 (4)	118.7
C ₂ –C ₁ –N ₁₀	119.9 (4)	120.4 (4)	120.4
C ₆ –C ₁ –N ₁₀	122.0 (4)	121.5 (4)	120.9
C ₁ –C ₂ –C ₃	119.7 (4)	122.0 (4)	119.8
C ₁ –C ₂ –H ₇	113.0 (2)	115.0 (3)	121.5
C ₃ –C ₂ –H ₇	128.0 (2)	125.0 (3)	118.7
C ₂ –C ₃ –C ₄	122.1 (5)	121.2 (5)	121.3
C ₂ –C ₃ –X ₁₃ ^a	124.0 (4)	122.0 (2)	119.4
C ₄ –C ₃ –X ₁₃ ^a	118.0 (4)	118.0 (2)	119.3
C ₃ –C ₄ –C ₅	117.6 (5)	119.2 (5)	119.4
C ₃ –C ₄ –X ₁₄ ^a	120.0 (3)	120.0 (3)	119.8
C ₅ –C ₄ –X ₁₄ ^a	123.0 (3)	121.0 (3)	120.8
C ₄ –C ₅ –C ₆	120.9 (5)	120.6 (5)	120.1
C ₄ –C ₅ –H ₈	115.0 (3)	118.0 (2)	118.9
C ₆ –C ₅ –H ₈	124.0 (3)	122.0 (2)	121.0
C ₁ –C ₆ –C ₅	121.8 (4)	121.1 (4)	120.7
C ₁ –C ₆ –H ₉	111.0 (3)	128.0 (3)	119.8
C ₅ –C ₆ –H ₉	127.0 (3)	111.0 (3)	119.5
C ₁ –N ₁₀ –H ₁₁	103.0 (4)	113.0 (4)	115.9
C ₁ –N ₁₀ –H ₁₂	124.0 (3)	121.0 (2)	115.6
H ₁₁ –N ₁₀ –H ₁₂	119.0 (4)	104.0 (5)	112.2
<i>Selected dihedral angles^b (°)</i>			
C ₂ –C ₁ –N ₁₀ –H ₁₁	–	–	–25.1
C ₂ –C ₁ –N ₁₀ –H ₁₂	–	–	–159.4
C ₆ –C ₁ –N ₁₀ –H ₁₁	–	–	157.9
C ₆ –C ₁ –N ₁₀ –H ₁₂	–	–	23.6

^a X = H or F, depending on the molecule.

^b A dihedral angle between the NH₂ plane and the ring plane.

normal value of 120°. The ring C–C–C, bond angles were observed in the range of 117.6–122.0° for aniline molecule [14]. As the discussion of the paper [53] for fluoroanilines, the calculated CCC angles in the aromatic ring, the structural changes are consistent with the σ electron-withdrawing (inductive) effect of the fluorine substituent at different sites of the ring.

If the substituted X (X; F, Cl, Br...) in place of hydrogen atom the bond length shows a remarkable increase. The C–F bond lengths were predicted at 1.348 and 1.352 Å, by using B3LYP/6-311G++(d,p) basis set in this paper and before bonding fluorine atoms were observed at ca. 1.05 Å for the structure of aniline [14]. The C–F bond lengths were also computed at 1.361, 1.352 and 1.356 Å for monofluoroaniline (2-, 3- and 4-FA) [53]. The C–F distance determined for fluorobenzene (1.354 ± 0.006 Å) by microwave spectroscopy [54]. The C–F bond lengths 1.348 Å for 2,4,5-TFA and 1.354 Å for 2,4,6-TFA and 1.366 Å for 4-FA were calculated [31] and also the experimental bond length observed at 1.363 Å for the C–F bond in 4-FA [55] i.e., the substituted two F atoms which are in the plane of benzene ring in the studied molecule in comparison to 4-FA interacted strongly with the F atom situated at para position with respect to amine group and diminished the magni-

tude of bond length of the C–F bond. Similar calculations [31,33,40,47,48,52,53] and observations [14,55] are seen in the literature for the structurally similar molecules.

Vibrational spectral analysis

This section gives to make a comparison with the results of the theoretical calculations with the experimental results and structurally similar molecules. Because of the helpful and realistic accommodation, spectroscopic signature and the assignment of the vibrational spectra were prepared for 3,4-DFA molecule. The theoretical results were performed by DFT/B3LYP/6-311G++(d,p) basis set, showed that higher than the experimental ones. The deviation can be a consequence of the anharmonicity and the general tendency of the quantum chemical methods to overestimate the force constants at the exact equilibrium geometry. The other plausibility is the theoretical results have obtained in vacuum, as otherwise experimental ones for liquid phase. To minimize the overall deviation, the calculated frequencies were scaled by the scale scaling factor [35]. The experimental (FT-IR and FT-Raman) and theoretical (with the scaling factor) vibrational spectra were presented in Figs. 2 and 3.

3,4-DFA molecule belongs to C₁ point group symmetry, consists of 14 atoms, so it has 36 fundamental vibrational modes (A species). In the C₁ point group symmetry of the title molecule is non-planar structure and has the 36 vibrational modes span the irreducible representations: 36. In the case of C_s point group symmetry of this molecule, there is an imaginary frequency (–410.36 cm^{–1}). Therefore we run program with C₁ point group symmetry. The experimental (FT-IR and FT-Raman) spectra and the calculated vibrational wavenumbers along with their assignments with PED of 3,4-DFA molecule are tabulated in Table 2.

NH₂ (amino group) modes

The molecule 3,4-DFA has a NH₂ group, has two (N–H) stretching vibrations, as asymmetric and symmetric stretching. Generally asymmetric vibration modes are recorded higher than that of symmetric ones. In primary amines, usually the N–H stretching vibrations occur in the region 3500–3300 cm^{–1} [18,56,57]. The N–H stretching modes also were presented at 3418–3515 cm^{–1} (vapor), 3401, 3485 cm^{–1} (solution) and 3360, 3440 cm^{–1} (liquid) for infrared and 3360, 3435 cm^{–1} (liquid) for Raman spectrum of aniline the base molecule of the studied molecule [10]. The asymmetric and symmetric vibrations of N–H stretching were recorded at 3460 and 3380 cm^{–1} respectively [58]. The two N–H bond stretching frequencies were observed at 3432, 3366 cm^{–1} in ortho-, 3440, 3376 cm^{–1} in meta- and 3425, 3370 cm^{–1} in para-fluoroanilines [26]. In the IR spectrum of aniline, the asymmetric and symmetric NH₂ stretching vibrations were assigned at 3508 and 3421 cm^{–1} respectively, also in para-fluoroaniline. These bands were observed at lower frequencies 3499 and 3414 cm^{–1} [28]. The frequencies of NH₂ were presented at 3393 and 3459 cm^{–1} (for 2,3,4-TFA) and 3387 and 3481 cm^{–1} (for 2,3,6-TFA) were assigned to the symmetric and asymmetric modes respectively, showed by their PEDs (ca. 100%) [30]. In the present case these modes are computed at 3423 and 3516 cm^{–1} symmetric and asymmetric modes respectively and observed at 3430 cm^{–1} (FT-IR) and 3372 cm^{–1} (FT-Raman) only symmetric modes for 3,4-DFA molecule. Brief looks above comment are showed that found to be in a good agreement. As expected these two modes are pure stretching modes as it is evident from PED column, they are almost contributing 100%.

The N–H scissoring modes are usually observed in the region 1610–1630 cm^{–1} [59]. According to the PED obtained for 4-FA, this vibration contributes to two modes, assigned two N–H scissoring bands, at 1620 and 1630 cm^{–1}, in the experimental IR spectrum of 4-FA [26]. The band observed in Raman spectrum at

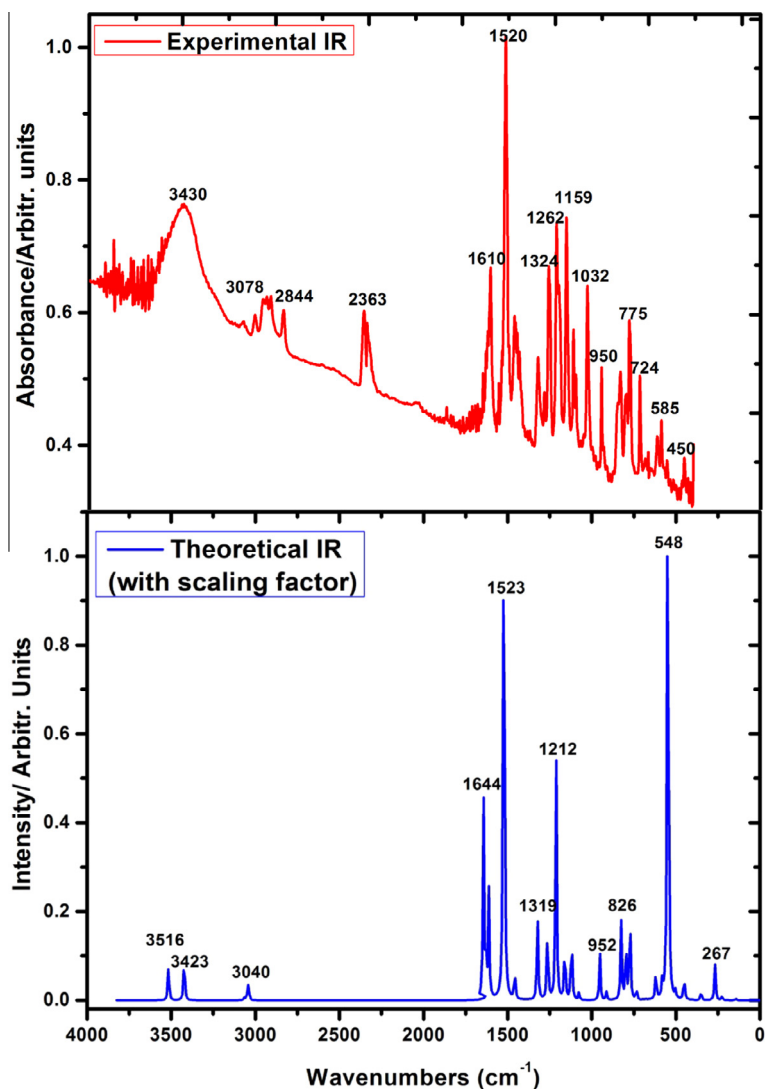


Fig. 2. The calculated (with the scale factor) and experimental infrared spectra of 3,4-DFA.

1689 cm^{-1} is assigned to NH_2 scissoring for 4-chloro-2-fluoroaniline molecule [60]. In this paper we computed at 1629 and 1644 cm^{-1} and recorded 1641 cm^{-1} (FT-IR) and 1629 cm^{-1} (FT-Raman), assigned N–H scissoring modes (ρNH_2). Also some modes were assigned δCNH but these modes are mixed modes with the other in plane and stretching modes. The mode number 17 which is contributed largest one according to their PED (49%). The δCNH mode was computed at 1076 cm^{-1} (1032 cm^{-1} in FT-IR) the largest contributions of them.

The wagging and torsional modes were assigned at 550 and 255 cm^{-1} for 2,3,4-TFA and 470 and 370 cm^{-1} for 2,3,6-TFA, respectively [30]. In the title molecule, the N–H wagging and torsional modes are predicted at 548 and 267 cm^{-1} respectively. According to the literature for structurally similar molecules [30–33,53,60], these assignments are agree well.

C–NH₂ modes

The C–NH₂ stretching frequency is rather difficult work since there are problems in identifying these frequencies from other vibrations [61]. Silverstein [59] assigned C–NH₂ stretching vibrations in the region 1386–1266 cm^{-1} for aromatic amines. In the infrared spectrum of liquid aniline the band of medium intensity at 1278 cm^{-1} was assigned to the C–NH₂ stretching mode [10].

In the experimental Raman spectrum of 4-FA, the ν (C–NH₂) stretching vibration was assigned at slightly lower frequency, 1274 cm^{-1} [23]. The C–NH₂ stretching frequencies were recorded in the region 1200–1300 cm^{-1} for ortho-, meta- and para-fluoroanilines [26]. Also the corresponding medium intensity band at 1273 cm^{-1} in IR spectrum of 4-FA (1275 cm^{-1} in Raman) should be assigned to C–NH₂ mode [53]. In this study the C–NH₂ stretching modes were computed at 1160 cm^{-1} (1159 cm^{-1} in FT-IR) and 1323 cm^{-1} (1324 and 1323 cm^{-1} in FT-IR and FT-Raman) however the modes are contaminated the other modes. The in-plane and out-of-plane bending C–NH₂ vibrations have also been identified and given in Table 2 for the present molecule. The assignments are supported by their PEDs.

C–F modes

The present molecule has two fluorine atoms which are added at meta- and para-position of aniline ring. The C–F stretching vibrations were contaminated with other vibrations especially ring modes, so, there is no pure. Also these modes sprawled broad band see Table 2, assigned the modes number ν_9 , ν_{11} , ν_{13-16} , ν_{18} , ν_{22} , ν_{23} . The largest percentages of the modes are ν_{15} and ν_{22} as %27 and %31. The largest modes were computed at 773 and 1160 cm^{-1} , observed at 775 cm^{-1} (FT-IR), 774 cm^{-1} (FT-Raman), and 1159 cm^{-1} (FT-IR).

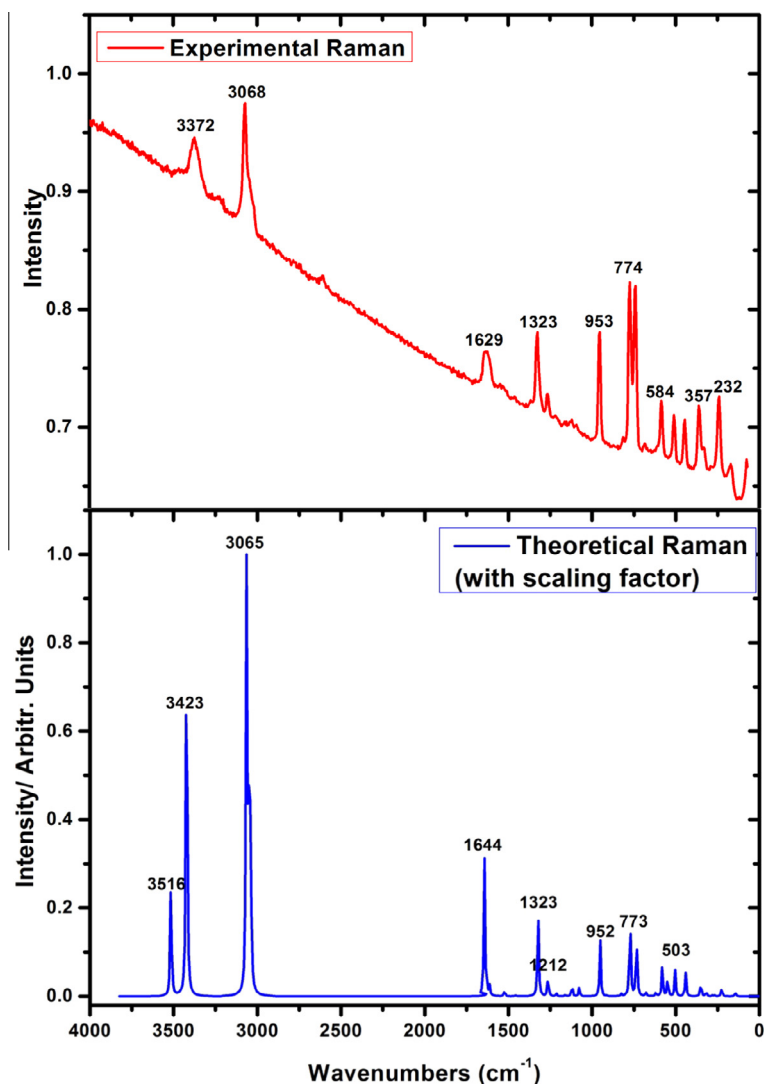


Fig. 3. The calculated (with the scale factor) and experimental Raman of 3,4-DFA.

Rastogi et al. [62] assigned the C–F stretching mode at 1250 cm^{-1} for tri- and tetra-fluoro benzene in infrared spectrum. Also this mode was observed at 1294 cm^{-1} (FT-IR) and 1298 cm^{-1} (FT-Raman) [63]. The C–F stretching vibration contributes predominantly mode were assigned to the strong and broad IR bands at 1206 cm^{-1} (2-FA) 1146 cm^{-1} (3-FA) and 1223 cm^{-1} (4-FA) and computed at 1194 , 1152 and 1223 cm^{-1} for 2-FA, 3-FA and 4-FA, respectively [53]. These modes were found in the range of 1232 and 1109 cm^{-1} for 2,4,5-TFA and 1353 and 1113 cm^{-1} for 2,4,6-TFA molecule [31]. The bands at 1210 and 998 cm^{-1} were assigned to the two C–F stretching vibrations for 2,5-DFA [64]. From the literature computations it turned out that only one frequency 980 cm^{-1} for 2,3,4-TFA and 1171 cm^{-1} for 2,3,6-TFA had very strong intensities in the IR spectrum whereas all the frequencies in the range of 1000 – 1350 cm^{-1} were found to have comparatively less intensities in the IR spectrum, but, with the help of PEDs were assigned at 1236 , 1020 and 980 cm^{-1} for 2,3,4-TFA and 1260 , 1041 and 924 cm^{-1} for 2,3,6-TFA to the three C–F stretching vibrations [30].

The in-plane C–F bending vibrations were found in the range of 266 – 318 cm^{-1} [65]. The frequency of one of three C–F in-plane bending modes was found at higher magnitude ca. 620 cm^{-1} [28] and ca. 595 cm^{-1} [30] for derivatives of substituted fluoroaniline molecules. Similarly, for several mono-fluoroanilines [26,64,66]

the frequency ca. 435 cm^{-1} had been assigned to the C–F in-plane bending vibration. In the present case, the frequencies of two of the five C–F in-plane bending modes were calculated at bigger magnitudes as 280 and 580 cm^{-1} also observed 585 and 584 cm^{-1} (FT-IR and FT-Raman). This view is supported by the above literature [28,30,31].

The modes of the C–F out-of-plane bending vibrations are assigned at 232 and 357 cm^{-1} in FT-Raman spectrum, computed at 225 and 350 cm^{-1} by DFT/B3LYP/6-311G++(d,p) basis set. In the previous work for fluorine substituted ring, the out-of-plane bending C–F modes were predicted at 291 and 204 cm^{-1} [67] and also observed at 377 cm^{-1} in FT-Raman [68]. Our results are also good consistency with in the previous literature [28,30,31]. The other bending and torsion modes of the related fluorine atom accounted in Table 2.

C–H modes

The poly peaks of the C–H stretching modes seem in the 3000 – 3100 cm^{-1} range, which is the typical region [69]. 3,4-DFA has three adjacent aromatic C–H units on benzene ring. The C2–H7, C5–H8, and C6–H9 stretching vibrations corresponds to modes no. 3, 4 and 5. In the current case, C–H stretching modes were predicted in the range of 3040 – 3065 cm^{-1} by using the

Table 2The comparison of the calculated harmonic frequencies and experimental (FT-IR and FT-Raman) wavenumbers (cm^{-1}) using by B3LYP method 6-311++G(d,p) basis set of 3,4-DFA.

Modes No.	Theoretical		Experimental		PED ^a (>10%)
	Unscaled freq.	Scaled freq.	FT-IR	FT-Raman	
v1	3670	3516			$\nu_{\text{NH}_{\text{asym}}}$ (100)
v2	3573	3423	3430	3372	$\nu_{\text{NH}_{\text{sym}}}$ (100)
v3	3199	3065	3078	3068	$\nu_{\text{CH}_{\text{sym}}}$ (100)
v4	3187	3053			$\nu_{\text{CH}_{\text{asym}}}$ (100)
v5	3174	3040	3016		$\nu_{\text{CH}_{\text{asym}}}$ (100)
			2967		Overtone/combination
			2942		Overtone/combination
			2914		Overtone/combination
			2844		Overtone/combination
			2363		Overtone/combination
			2343		Overtone/combination
v6	1672	1644	1641		ν_{CC} (39), ρ_{NH_2} (29), δ_{CCC} (11)
v7	1657	1629		1629	ρ_{NH_2} (35), ν_{CC} (23)
v8	1640	1612	1610		ν_{CC} (66), δ_{CCC} (21)
v9	1549	1523	1520		δ_{CCH} (40), δ_{CCC} (23), ν_{CF} (12), ν_{CC} (12)
v10	1483	1458	1462		ν_{CC} (35), δ_{CCH} (26)
v11	1346	1323	1324	1323	ν_{CC} (38), $\nu_{\text{C-NH}_2}$ (28), ν_{CF} (18)
v12	1342	1319	1293		ν_{CC} (81), δ_{CNH} (11)
v13	1285	1263	1262	1263	δ_{CCH} (52), ν_{CC} (23), ν_{CF} (14)
v14	1233	1212	1213		δ_{CCH} (36), δ_{CCC} (24), ν_{CF} (20)
v15	1180	1160	1159		δ_{CCH} (40), ν_{CF} (27), ν_{CC} (21), $\nu_{\text{C-NH}_2}$ (12)
v16	1139	1120	1117	1118	δ_{CCH} (38), ν_{CF} (16), ν_{CC} (15), δ_{CCC} (14), δ_{CNH} (12)
v17	1095	1076	1032		δ_{CNH} (49), ν_{CC} (25), δ_{CCH} (15)
v18	969	952	950	953	δ_{CCC} (50), δ_{CCH} (18), ν_{CF} (14), ν_{CN} (11)
v19	929	913			γ_{CH} (98)
v20	840	826	829		γ_{CH} (95)
v21	811	797	800		γ_{CH} (96)
v22	787	773	775	774	ν_{CC} (42), ν_{CF} (31), δ_{CCC} (19)
v23	747	734	724	736	δ_{CCC} (58), ν_{CC} (18), ν_{CF} (12)
v24	690	678	672	681	τ_{CCCC} (33), τ_{CCCF} (37), τ_{CCCN} (15), τ_{CCNH} (14)
v25	629	619	617		τ_{CCCN} (42), τ_{CCCN} (30), τ_{CCNH} (22)
v26	590	580	585	584	δ_{CCF} (52), δ_{CCC} (23), ν_{CC} (12), δ_{CCN} (11)
v27	557	548	556		ω_{NH} (76), δ_{NH_2} (11)
v28	511	503		507	δ_{CCC} (30), δ_{CCF} (17), ν_{CC} (16), δ_{CCN} (13)
v29	459	451	450		τ_{CCCC} (50), τ_{CCNH} (30), τ_{CCCF} (21)
v30	449	441		443	δ_{CCC} (68), δ_{CCF} (18)
v31	356	350		357	τ_{CCCF} (62), τ_{CCCC} (31)
v32	323	318			δ_{CCN} (52), δ_{CCF} (22), ν_{CC} (20)
v33	285	280			δ_{CCF} (81)
v34	272	267			τ_{NH} (92)
v35	229	225		232	γ_{CF} [τ_{CCCC} (59), τ_{CCCF} (27)]
v36	146	144		169	τ_{CCCC} (82)

^a PED: potential energy distribution; ν : stretching; γ : out-of plane bending; δ : in-plane-bending; τ : torsion; ρ : scissoring; ω : wagging.

DFT/B3LYP/6-311++G(d,p) method and recorded at 3016, 3078 cm^{-1} (FT-IR) and 3068 cm^{-1} (FT-Raman) respectively. The PED contribution of these modes also was presented very pure 100%. In these results showed that the C–H bands of are not affected appreciably by the nature of the substituents. The C–H stretching modes of the base structure of the title molecule (aniline) were chronicled in the region 3025–3094 cm^{-1} (vapor), 3013–3094 cm^{-1} (solution) 3010–3088 cm^{-1} (liquid) in infrared spectrum and 3010–3072 cm^{-1} (liquid) in Raman spectrum, respectively [10]. Also Badawi et al. [70] recorded at 3035–3106 cm^{-1} in FT-IR and 3054–3109 cm^{-1} in FT-Raman spectra for aniline molecule. The frequencies were also recorded for many derivatives of aniline molecules such as: at 3096 and 3073 cm^{-1} and at 3091 cm^{-1} for 2,4,5-TFA and 2,4,6-TFA, respectively, which consists of a doublet [31], ca. 3033–3066 cm^{-1} , 3025–3065 cm^{-1} (FT-IR) 3010–3069 cm^{-1} (FT-Raman) for para-halogenoanilines [33], 3107 cm^{-1} infrared spectrum for structurally similar molecule 2,3-DFA [29] and the same region for mono-fluoroaniline isomers [53].

The in plane and out-of-plane bending C–H vibrations record in the range of 1000–1300 cm^{-1} and 750–1000 cm^{-1} , respectively [69]. The region of 1028–1180 cm^{-1} (vapor), 1028–1308 cm^{-1} (solution) 1028–1312 cm^{-1} (liquid) in infrared spectrum and 1029–1176 cm^{-1} (liquid) in Raman spectrum, respectively were

assigned as in plane bending C–H vibrations, also the out-of-plane bending C–H vibrations were observed in the region 740–874 cm^{-1} (vapor), 747–968 cm^{-1} (solution) 751–970 cm^{-1} (liquid) in infrared spectrum, and 755–970 cm^{-1} (liquid) in Raman spectrum respectively by Evans in 1960 for aniline molecule [10]. In the current paper, the in plane C–H vibrations were predicted at 952–1523 cm^{-1} and observed at 950–1520 cm^{-1} in FT-IR spectrum and 953–1323 cm^{-1} in FT-Raman for 3,4-DFA molecule and the out-of-plane bending calculated at 797, 826 and 913 cm^{-1} and observed at 800 and 829 cm^{-1} in FT-IR spectrum for the title molecule. As seen Table 2 clearly the C–H in-plane modes are generally coupled or contaminated the CC stretching modes. Withal the literature results showed well concordance with the experimental and theoretical paper for the structurally similar compound [26–28,30,31,53,58,64,66] our results shows very good correlation for monomer and dimer structure of the studied molecule. The change in the frequencies of these C–H vibrations from the values in benzene is determined mainly by the relative position of the substituents.

C–C modes

The modes of C–C stretching are very significant for the aromatic ring and also highly characteristic. Varsanyi [71] gave that the

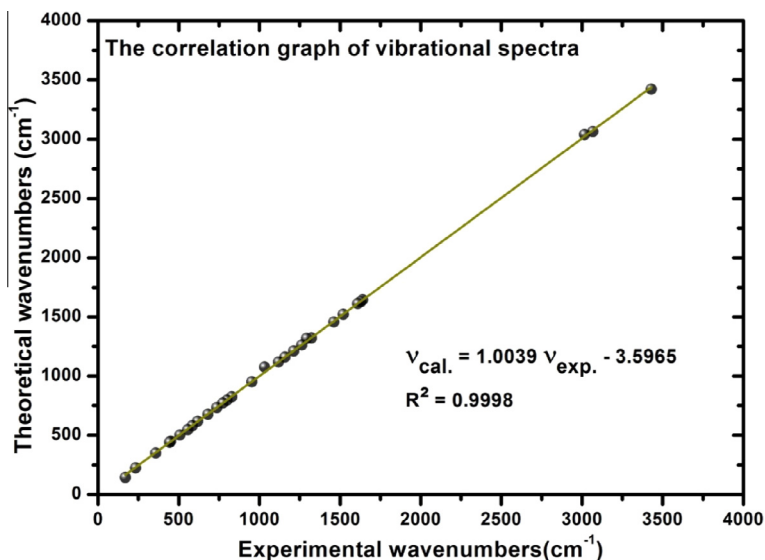


Fig. 4. The correlation graphic of the calculated and experimental frequencies of 3,4-DFA.

bands were of variable intensity and were observed at 1625–1590, 1590–1575, 1540–1470, 1465–1430 and 1380–1280 cm^{-1} from the frequency ranges for the five bands in the region. The C–C stretching modes were computed in the region 1644–1263, 1160–952, 773, 734, 580, 503 and 318 cm^{-1} for the title molecule. The observed values are 1641–1262, 1159–950, 775, 724 and 585 cm^{-1} in FT-IR spectrum and 1629–1263, 1118–953, 774, 736, 584 and 507 cm^{-1} in FT-Raman spectrum in the headline molecule. The largest contribution of C–C stretching vibrations come from 1319 cm^{-1} (%81) and 1612 cm^{-1} (%66), assigned nearly pure modes of 3,4-DFA molecule. Similar papers [26–28,30,31,53,58,64,66] were supported in our present molecule, showing good correlations.

The CCC bending (as seen ring deformation) and torsion modes were meddled with other modes and sometimes missing in FT-Raman spectrum. The two biggest and purest contribution of CCC bending modes (ν_{30}) were recorded at 443 cm^{-1} FT-Raman and the other (ν_{23}) 736 cm^{-1} in FT-Raman and 724 cm^{-1} in FT-IR, calculated wavenumbers of these modes coincide at 441 and 734 cm^{-1} with scaling factor. The torsion modes were assigned in the broad band and contaminated other modes and also named as out-of plane modes of C–H or N–H. So, these modes are not discussed here.

To show coherent between the experimental and calculated frequencies the correlation graphic was plotted and presented in Fig. 4 considering both infrared and Raman spectra. Also the correlation graphics for infrared and Raman were graphed one by one as Fig. S2a and b. The relations of wavenumbers are described as linear for total and one by one (infrared and Raman) the under given equations:

$$v_{\text{cal.}} = 1.0039 v_{\text{exp.}} - 3.5965 \quad (\text{Total-}R^2 = 0.9998)$$

$$v_{\text{cal.}} = 0.9995 v_{\text{exp.}} + 4.1595 \quad (\text{Infrared-}R^2 = 0.9998)$$

$$v_{\text{cal.}} = 1.0116 v_{\text{exp.}} - 12.758 \quad (\text{Infrared-}R^2 = 0.9999)$$

NMR spectra

NMR spectra are one of important techniques in order to the structural analysis for organic compounds. To interpret and predict the even structure of large biomolecules the NMR spectroscopic technique and computer simulation methods offers a powerful

way with together [72]. The NMR spectral computations are predicted by using GAUSSIAN 09W [38] package program. The ^1H and ^{13}C NMR spectra were employed because of the utility practical and extensive for providing the more information about the headline molecule. So ^1H and ^{13}C NMR analysis were performed both experimentally and theoretically for 3,4-DFA molecule. The experimental ^1H and ^{13}C NMR spectra of the title molecule were presented in Fig. 5a and b, respectively. The experimental and theoretical data of the spectra of ^1H and ^{13}C NMR in chloroform-d (CDCl_3) solution solvent were served up in Table 3. The atom positions were arranged based on number of Fig. 1.

To take theoretical NMR chemical shifts of the molecule, the full geometry optimization of 3,4-DFA molecule was performed by using the DFT/B3LYP/6-311G++(d,p) basis set. After optimization, the GIAO [44,45] method were exploited for ^1H and ^{13}C NMR calculations. Due to the GIAO approach to molecular systems was essentially developed by an efficient application method of ab-initio SCF calculations, by using techniques taken from analytic derivative methodologies [44,45].

The relative chemical shifts are estimated by using the respective TMS shielding calculated in advance at the theoretical level as reference. The changes in energy necessitated to flip protons are called chemical shifts. The location of chemical shifts (peaks) on NMR spectrum is measured from a reference point that the hydrogen in a standard reference compound TMS produce.

The studied molecule has five hydrogen atoms. The hydrogen atoms of the studied molecule were divided into two groups (NH_2 and ring). The aromatic ring protons of organic molecules usually have in the range of 7.00–8.00 ppm chemical shifts. The proton chemical shifts change widely with the electronic environment. Electron-withdrawing atom or group (hydrogen attached or nearby) can decrease the shielding and move the resonance of attached proton towards to a higher frequency, while electron-donating a lower frequency [73]. The calculated parameters were compared to the experimental characteristics of the title compound. The calculated proton chemical shifts were sorted at 6.57, 7.04, 6.44 ppm in the benzene ring. The recorded experimental values were in the region parts as 6.30–6.94 ppm. The chemical shifts value of H_8 greater than other ring protons, due to the electronic environment of nearby of F_{14} atom. But the chemical shifts obtained and calculated for the hydrogen atoms of amino groups are quite low. Two signals result from NH_2 group (H_{11} and H_{12}) were observed as combined one peak as a coupling (3.57 ppm)

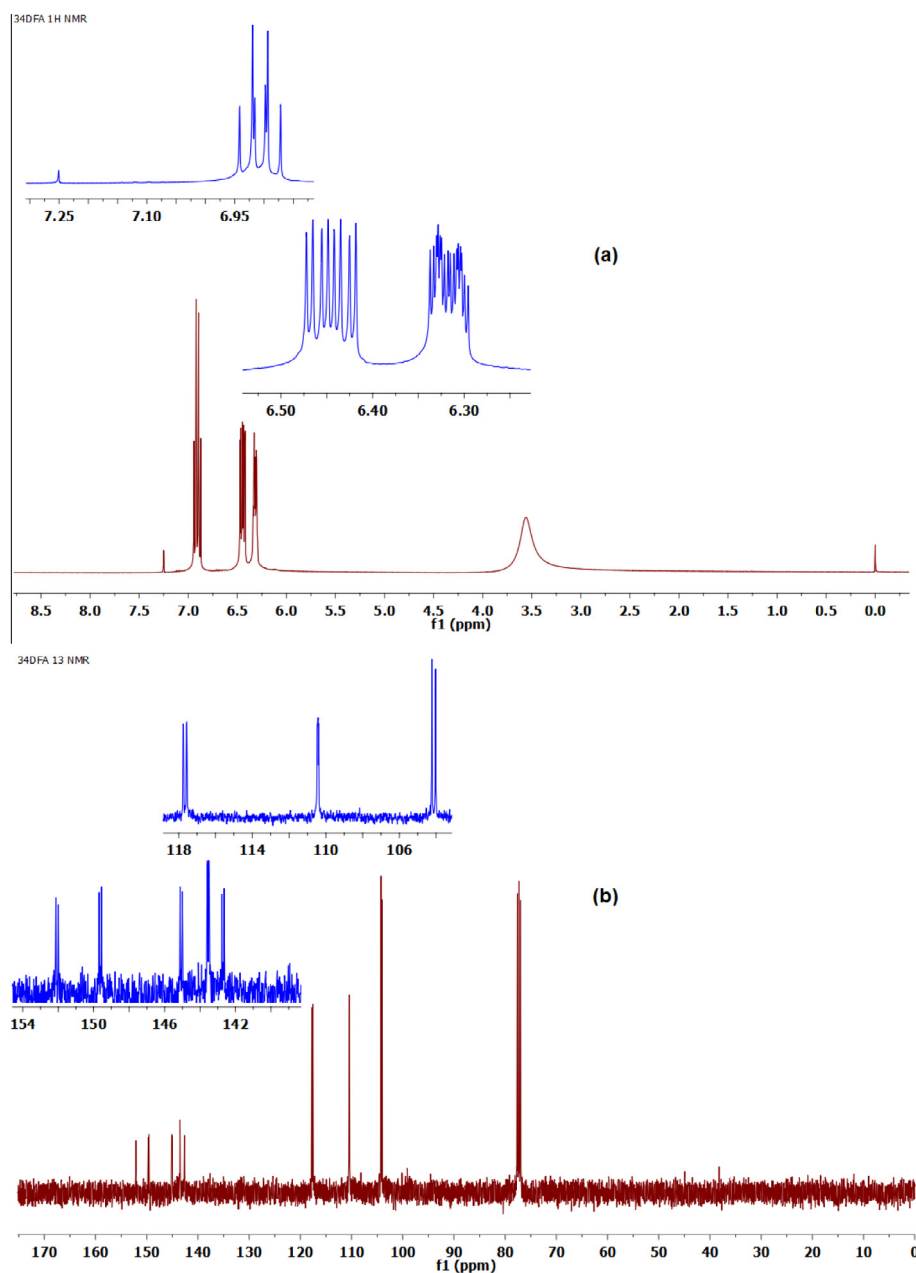


Fig. 5. (a) ¹H NMR (b) ¹³C NMR spectra of 3,4-DFA in chloroform-d solution.

which calculated at 3.36 and 3.40 ppm attached electron-withdrawing atom (N) can decrease the shielding, determined by using B3LYP/6-311++G(d,p) method.

The chemical shift values of aromatic carbons give resonances in overlapped areas of the NMR spectrum with from 100 to 150 ppm [74,75]. The carbon atoms in the ring for 3,4-DFA molecule were the same parallel with this range and well agreement. The carbon chemical shifts of 3,4-DFA molecule were computed at 105.76, 112.50, 122.27, 150.18, 150.85, 158.82 ppm and observed in the range of 104.03–152.13 ppm. The C₂, C₅ and C₆ atoms have smaller chemical shifts (both experimental and theoretical) than the other ring carbon atoms, due to electronic environment of N and F atoms. The C₁, C₃ and C₄ atoms have the biggest chemical shift values, because of the attached electron-withdrawing atoms (F or N atoms). The carbon atom (C₃) resonance at lower field, and the signal of this carbon atom was recorded at 149.56–152.13 and calculated at 158.82 ppm. If the literature the results

were detected the chemical shift of the present molecule were well consistency for the this structurally similar molecules [60,61,76].

Fig. 6 hustled up to demonstrate coherent of between the experimental and calculated chemical shifts of 3,4-DFA molecule. The average values used for the correlation graphs. ¹H and ¹³C NMR correlation graphics were presented one by one in Figs. S3 and S4, respectively. Moreover the underrepresented equations show the relations between the experimental and calculated chemical shifts:

$$\text{Total} : \delta_{\text{cal.}} (\text{ppm}) = 1.0447\delta_{\text{exp.}} - 0.5184 \quad (R^2 = 0.9996)$$

$$^1\text{H} : \delta_{\text{cal.}} (\text{ppm}) = 1.1030\delta_{\text{exp.}} - 0.5516 \quad (R^2 = 0.9971)$$

$$^{13}\text{C} : \delta_{\text{cal.}} (\text{ppm}) = 1.1303\delta_{\text{exp.}} - 11.750 \quad (R^2 = 0.9994)$$

Table 3

Experimental and theoretical, ^1H and ^{13}C NMR isotropic chemical shifts (with respect to TMS) of 3,4-DFA with DFT (B3LYP 6-311++G(d,p)) method.

Atoms Carbon			Atoms Hydrogen		
No.	Experimental	Theoretical	No.	Experimental	Theoretical
C(1)	142.64–145.12	150.85	H(7)	6.30–6.34	6.57
C(2)	104.03–104.23	105.76	H(8)	6.87–6.94	7.04
C(3)	149.56–152.13	158.82	H(9)	6.42–6.47	6.44
C(4)	143.48–143.60	150.18	H(11)	3.57	3.36
C(5)	117.56–117.76	122.27	H(12)	3.57	3.40
C(6)	110.38–110.48	112.50			

The ^{13}C NMR results gave a slightly better coefficient and lower standard error ($R^2 = 0.9994$) than for ^1H ($R^2 = 0.9971$) chemical shifts. The ^1H and ^{13}C chemical shifts data, collected in Table 3, are described fairly well correlation. However, very small deviation between experimental and theoretical protons can be due to the solvent effects.

Electronic properties

UV–Vis spectrum and frontier molecular orbital analysis

The UV–Vis (electronic absorption) spectra of the title molecule were saved in ethanol and water at room temperature experimentally and theoretically. TD–DFT results of the electronic absorption spectrum are a quite reasonable method and computationally more expensive than semi-empirical methods but allow easily studies of medium size molecules [77,78]. The theoretical and experimental UV–Vis spectra of the steady molecule are illustrated in Fig. 7. The experimental parameters are compared to the calculated characteristics of 3,4-DFA molecule. The values are observed at 216.86, 277.11 nm (ethanol) and 209.11, 273.51 nm (water) experimentally. The calculated values are 234.17, 244.55 and 272.96 nm (ethanol), 234.38, 244.03 and 272.93 nm (water) with TD–DFT/B3LYP/6-311++G(d,p) basis set both two solutions. The wavelengths (λ), excitation energies (E), oscillator strengths (f), and calculated counterparts with major contributions can be seen in Table 4 for two solutions and gas phase.

The primary frontier molecular orbitals (FMOs) such that highest occupied molecular orbital (HOMO) and lowest unoccupied molecular orbital (LUMO) play an important role in the electric and optical properties. The HOMO and LUMO have the ability of

electron giving and accepting characterizes, respectively. The energy gap of HOMO–LUMO refers to the potential energy difference between the HOMO and LUMO. Basically, it is how much energy has to be fed into the molecule to kick it from the ground state (the most stable) into an excited state [60]. To show surfaces of important the frontier orbitals (HOMO, LUMO, LUMO + 1, LUMO + 2 and LUMO + 3) and energy gaps were given in Fig. 8. The gap of energy were calculated 5.27 eV for HOMO and LUMO. The other important energy gaps of FMOs of 3,4-DFA molecule were gathered in Table 5. The HOMO and LUMO orbital, have the positive phase is red and the negative one is green nodes. The charge density of HOMO localized all of the molecule expect, but the LUMO is characterized by a charge distribution in the ring. The HOMO and LUMO energy computed by TD–DFT/B3LYP/6-311++G(d,p) method and the energy gap is given under given;

$$\text{HOMO}_{\text{energy}} (\text{B3LYP}) = -6.11 \text{ eV}$$

$$\text{LUMO}_{\text{energy}} (\text{B3LYP}) = -0.84 \text{ eV}$$

$$\text{HOMO} - \text{LUMO}_{\text{energy gap}} (\text{B3LYP}) = 5.27 \text{ eV}$$

Moreover the energy gaps of FMOs, between $\text{H} \rightarrow \text{L}$, $\text{H} \rightarrow \text{L} + 1$, $\text{H} \rightarrow \text{L} + 2$ and $\text{H} \rightarrow \text{L} + 3$ orbital, are a critical parameter in determining molecular electrical transport properties. The energy gaps ($\text{H} \rightarrow \text{L}$, $\text{H} \rightarrow \text{L} + 1$, $\text{H} \rightarrow \text{L} + 2$ and $\text{H} \rightarrow \text{L} + 3$) were computed 5.27, 5.64, 5.94 and 6.14 eV for gas phase for the title molecule. These values were also calculated in two solvents of the studied molecule given in Table 5. The molecular orbital orient 3,4-DFA molecule to see energy levels of molecular orbitals and some important energy gaps with their energy levels are given in Fig. S5.

Moreover the values of chemical hardness, electronegativity, chemical potential and electrophilicity index are compared for gas phase, in ethanol and water solutions in Table 5. The HOMO and LUMO energies were used to calculate the chemical hardness (η), electronegativity (χ), chemical potential (μ), and electrophilicity index (ω). The chemical hardness (η) and potential (μ) are good indicators of the chemical stability of molecular systems [60]. Electrophilicity index is a measure of energy lowering due to maximal electron flow between acceptor and donor. Parr and Chattaraj [79] proved the chemical hardness received much attention after the invention of Pearson's MHP, which states that

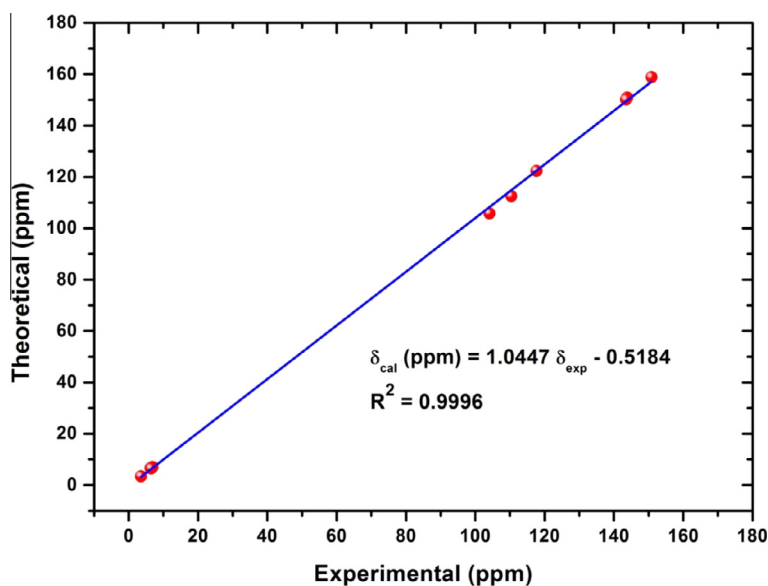


Fig. 6. The correlation graphic of the calculated and experimental (total) chemical shifts of 3,4-DFA.

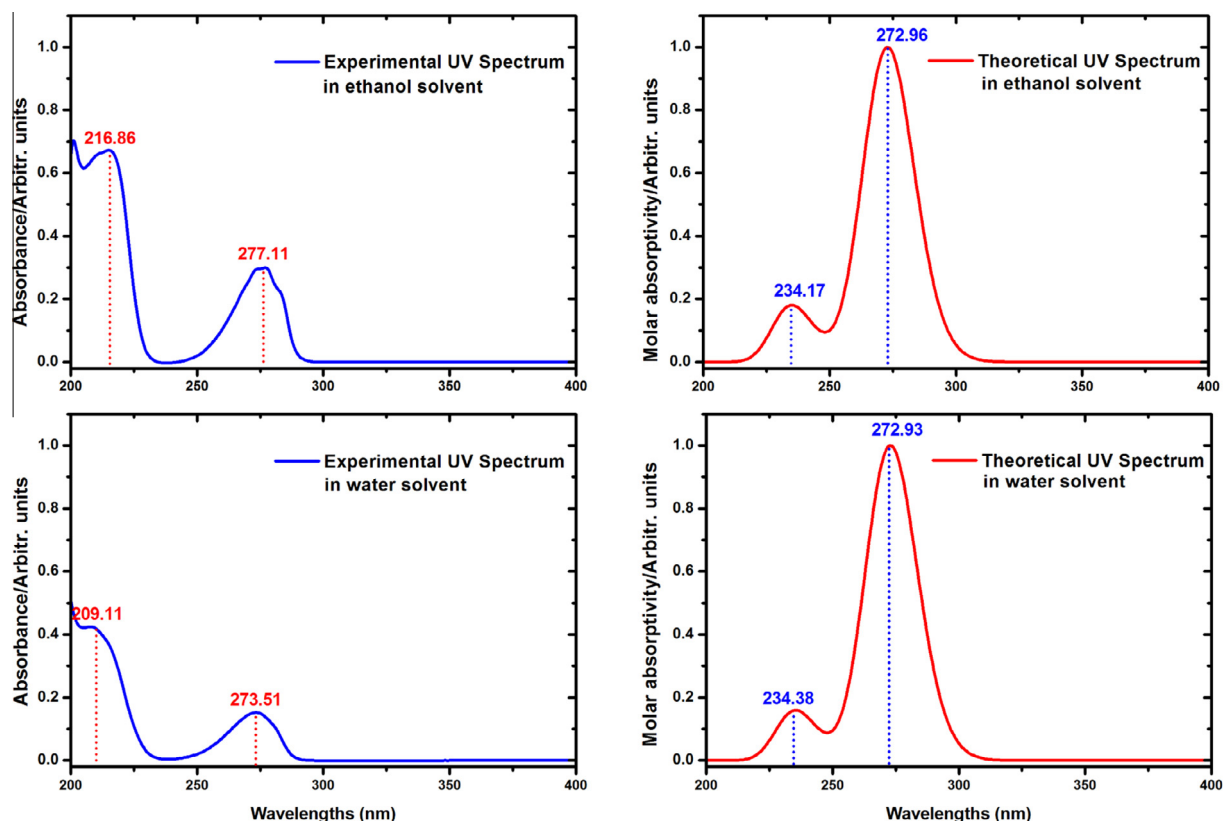


Fig. 7. The experimental and theoretical UV-Vis spectra of 3,4-DFA in ethanol and water.

Table 4

Experimental and calculated wavelengths λ (nm), excitation energies (eV), oscillator strengths (f) of 3,4-DFA gas phase, in ethanol and water solutions using TD-DFT/B3LYP/6-311++G(d,p).

λ (nm)	E (eV)	f	Major contributes	λ (nm)	E (eV)
<i>Gas</i>					
270.32	4.5872	0.0453	H \rightarrow L (90%)	–	–
262.63	4.7214	0.0046	H \rightarrow L + 1 (97%)	–	–
229.80	5.396	0.0039	H \rightarrow L + 3 (91%)	–	–
<i>Ethanol</i>					
272.96	4.5427	0.0588	H \rightarrow L (92%)	Exp. (ethanol)	4.4748
244.55	5.0706	0.002	H \rightarrow L + 2 (62%), H \rightarrow L + 1 (35%)	277.11	
234.17	5.2952	0.0097	H \rightarrow L + 3 (83%)	216.86	5.718
<i>Water</i>					
272.93	4.54321	0.0578	H \rightarrow L (92%)	Exp. (water)	4.5337
244.03	5.08128	0.0018	H \rightarrow L + 2 (72%), H \rightarrow L + 1 (26%)	273.51	
234.38	5.29051	0.0083	H \rightarrow L + 3 (84%)	209.11	5.9299

the minimum energy structure has the maximum hardness. The hard molecule is less polarizable than the soft one because it needs big excitation energy. In the present paper, the chemical hardness η of the title molecule is smaller than 3 eV while electronegativity (χ) is bigger than 3 eV. Also the chemical hardness is 2.64 eV for gas phase, 2.62 eV in ethanol and water solvents. The chemical hardness is decreasing 0.02 eV in solvents in the studied molecule. Electrophilicity index is a measure of energy lowering due to maximal electron flow between donor and acceptor. The electronegativity, chemical potential and electrophilicity index are also the same behavior in the solvents.

Total, partial, and overlap population density of states

The neighboring orbitals may show quasi degenerate energy levels in the boundary region. The HOMO and LUMO may not yield a realistic description of the frontier orbitals thereof the TDOS,

PDOS, and OPDOS (or COOP) density of states [80–82], were computed and created by convoluting the molecular orbital information with Gaussian curves of unit height and Full width at half maximum (FWHM) of 0.3 eV using the GaussSum 2.2 program [46] in point of the Mulliken population analysis. The bonding, anti-bonding and nonbonding natures of the interaction of the two orbitals, atoms or groups are showed OPDOS (COOP) diagrams. The positive and negative values indicate a bonding and an anti-bonding interaction also zero value indicates nonbonding interactions, respectively [83]. Additionally, the OPDOS diagram allows us to the determination and comparison of the donor-acceptor properties of the ligands and ascertain the bonding, non-bonding.

The PDOS, TDOS and OPDOS of the molecule were graphed and given in Figs. 9 and S6–S7, respectively. The PDOS mainly gives the composition of the fragment orbitals contributing to the molecular

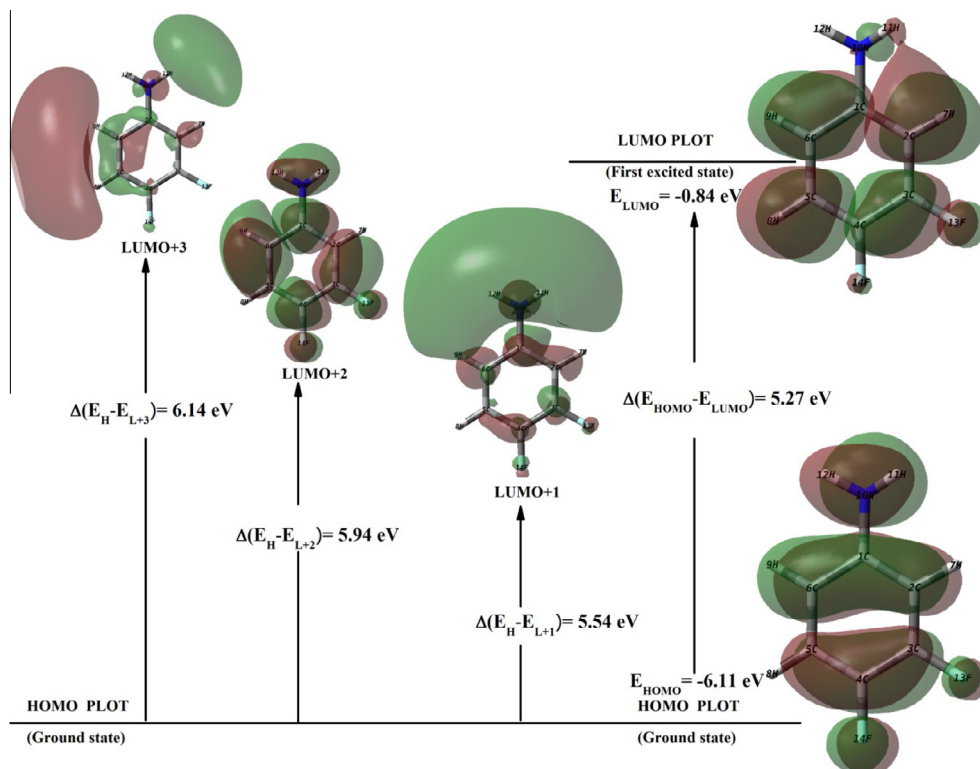


Fig. 8. The selected frontier molecular orbitals of 3,4-DFA with the energy gaps.

Table 5

The calculated energies values of 3,4-DFA molecule using by the TD-DFT/B3LYP method using 6-311++G(d,p) basis set.

TD-DFT/B3LYP/6-311++G(d,p)	Gas	Ethanol	Water
E_{total} (Hartree)	-486.0484948	-486.058419	-486.058799
E_{HOMO} (eV)	-6.11	-6.06	-6.06
E_{LUMO} (eV)	-0.84	-0.82	-0.82
$E_{\text{LUMO}+1}$ (eV)	-0.57	-0.21	-0.20
$E_{\text{LUMO}+2}$ (eV)	-0.17	-0.14	-0.14
$E_{\text{LUMO}+3}$ (eV)	0.03	0.08	0.08
$E_{\text{HOMO-LUMO}}$ gap (eV)	5.27	5.24	5.24
$E_{\text{HOMO-LUMO}+1}$ gap (eV)	5.54	5.85	5.86
$E_{\text{HOMO-LUMO}+2}$ gap (eV)	5.94	5.92	5.92
$E_{\text{HOMO-LUMO}+3}$ gap (eV)	6.14	6.14	6.14
Chemical hardness (η)	2.64	2.62	2.62
Electronegativity (χ)	3.48	3.44	3.44
Chemical potential (μ)	-3.48	-3.44	-3.44
Electrophilicity index (ω)	2.29	2.26	2.26

orbitals. The HOMO orbital separated on phenyl ring, fluorine atoms and NH_2 group, their contributions 100%. The LUMO localized on the phenyl ring (96%), and NH_2 group (2%) of the title molecule. However, the percentage sharing of atomic or molecular orbitals in the molecule is very hard work to determine bonding and anti-bonding character. So we can use the OPDOS diagram and some of its orbitals of energy values of interaction between selected groups which are shown from figure easily. NH_2 group \leftrightarrow fluorine atoms (blue line) system is near the zero (non-bonding interaction) as well as ring (phenyl group) \leftrightarrow NH_2 group systems (red line) and ring \leftrightarrow fluorine atoms (black line). The OPDOS plots of the current molecule have bonding character in frontier HOMO and LUMO molecular orbitals for ring and fluorine atoms also NH_2 group.

Molecular electrostatic potential surface

The MEP surface diagrams of molecules are used to know the reactive behavior of the molecules, in that negative regions can be regarded as potential electrophilic sites, whereas the positive regions are nucleophilic centers, indicated as red and blue color, respectively. The molecular electrostatic potential is related to the electronic density and a very useful descriptor for determining sites for electrophilic attack and nucleophilic reactions as well as hydrogen-bonding [60,84,85]. 3D plots and 2D contour plots of the MEPs of the studied molecule are plotted and illustrated in Fig. 10. The values of the electrostatic potential at the surface increase in the order red < orange < yellow < green < blue in the map of MEPs. The color code line up range between -5.254×10^{-2} a.u. (red) and 5.254×10^{-2} a.u. (blue) in compound, where blue indicates the strongest attraction and red indicates the strongest repulsion. Negative regions are usually associated with the lone pair of electronegative atoms. As seen the MEPs map of the title molecule while regions having the negative potential are over the electronegative atoms (fluorine atoms), positive ones are over the hydrogen atoms especially attached NH_2 group (see Fig. 10). To show the values in an assortment of spatial site around the molecule the sliced 2D MEPs contour map of 3,4-DFA molecule are also represented that provide more exhaustive information regarding molecular electrostatic potential distribution. The around of the fluorine atoms have electron rich region and all the around of hydrogen atoms correspond to the electron deficient region (especially H atoms of amino group). In the 2D MEPs contour map, the maximum values of negative and positive potential corresponding to the nucleophilic and electrophilic region are -0.04 a.u. and 0.8 a.u. respectively.

Mulliken atomic charges

The Mulliken atomic charges of aniline and 3,4-DFA molecules are listed in Table S1 and also illustrated in Fig. S8. To have the

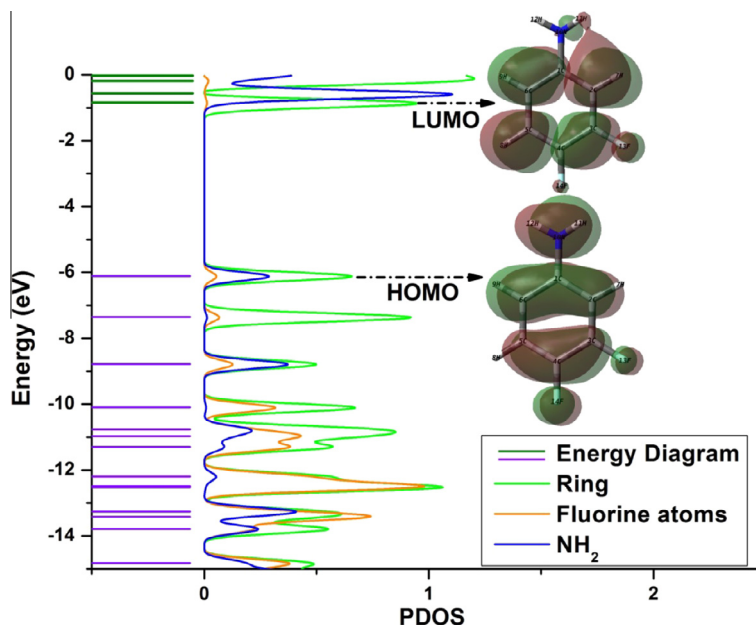


Fig. 9. The partial electronic density of states diagram of 3,4-DFA.

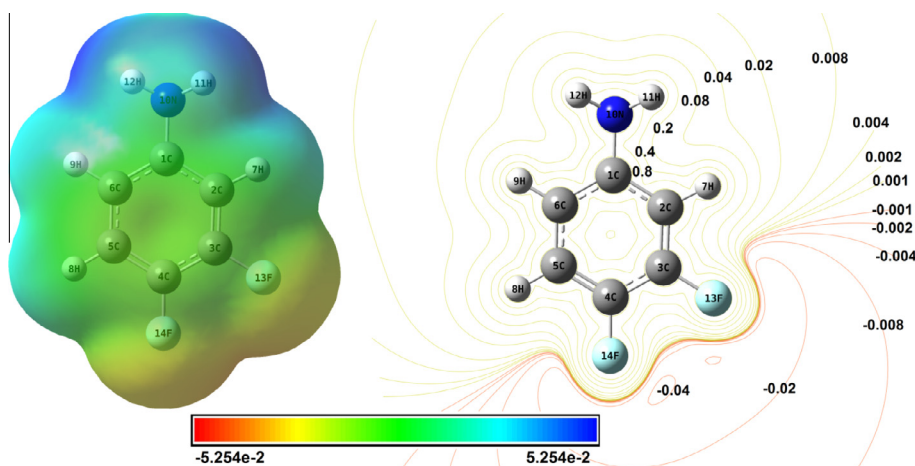


Fig. 10. The molecular electrostatic potential 3D map and 2D contour map for 3,4-DFA.

Mulliken atomic charges the DFT/B3LYP method 6-311++G(d,p) basis set are based on. By virtue of the reactive atomic charges play an important role in the application of quantum mechanical calculations the molecular system. The results indicate that fluorine atoms lead to a redistribution of electron density of aromatic ring for 3,4-DFA molecule. The charge of NH_2 group is the same distribution (negative or positive) and nearly the same magnitude for two molecules, but aromatic ring of the molecules exhibits a different charge with each other. As seen in Fig. S8 the charges of C_1 , C_2 , C_5 , and C_6 are negative for the aniline and however they are positive for 3,4-DFA molecule, due to the effect of the fluorine atoms and NH_2 group. The hydrogen atoms have a positive charge, which is an acceptor atom for both molecules.

Thermodynamic properties

The heat capacity (C), entropy (S), and enthalpy changes (ΔH) (statically thermodynamic functions) of 3,4-DFA molecule are obtained, to see the change of thermodynamic functions with the increasing temperature from 100 to 700 K, from the theoretical

harmonic frequencies according to vibrational analysis and tabulated in Table S2, due to the fact that the molecular vibrational intensities increase with temperature. The equations of correlation graphed between temperatures and heat capacity, entropy, enthalpy changes were fitted by quadratic formulas and the corresponding fitting factors (R^2). The relations between temperature and these thermodynamic properties are designed in Fig. S9. R^2 values are 0.9999, 0.9999 and 0.9997 for heat capacity, entropy, enthalpy changes, respectively. The corresponding fitting equations are given under:

$$C = -1.16163 + 0.12133T - 6.3813 \times 10^{-5}T^2 \quad (R^2 = 0.9999)$$

$$S = 50.25682 + 0.12657T - 3.5076 \times 10^{-5}T^2 \quad (R^2 = 0.9999)$$

$$\Delta H = -0.55765 + 0.00949T + 3.5438 \times 10^{-5}T^2 \quad (R^2 = 0.9997)$$

Last of all to supply helpful information for the further study on 3,4-DFA, the thermodynamical data were obtained. To calculate the other thermodynamic energies according to relationships of

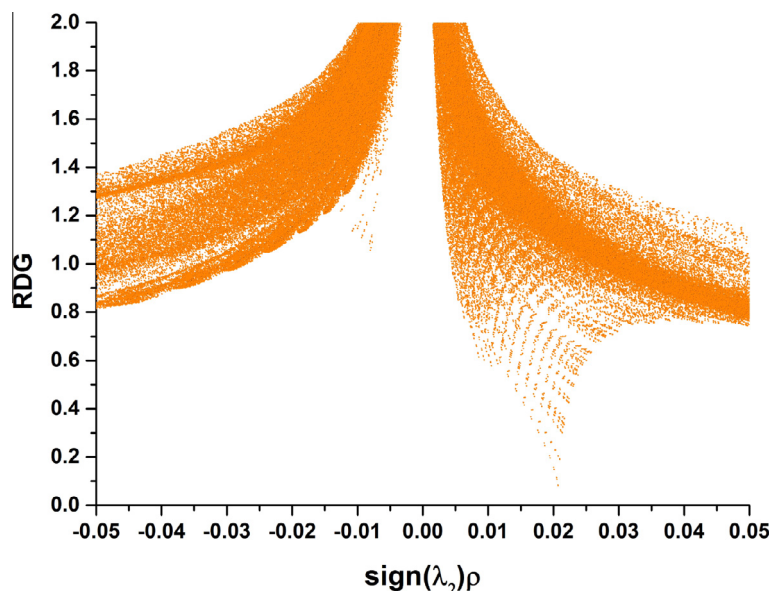


Fig. 11. Plots of the RDG versus the electron density ρ multiplied by the sign of λ_2 of 3,4-DFA.

thermodynamic functions and estimate directions of chemical reactions according to the second law of thermodynamics in Thermochemical field can be used. Notice: they were done for gas phase and could not be used in solution.

Nonlinear optical properties and dipole moment

The NLO properties such as: dipole moment, molecular polarizability, anisotropy of polarizability and molecular first hyperpolarizability of the title molecule were also proved in this study. To obtain the polarizability and hyperpolarizability tensors of 3,4-DFA molecule a frequency job output file of Gaussian are used. But, the units of α and β values of Gaussian output are converted into from in atomic units (a.u.) to electronic units (esu) (α ; 1 a.u. = 0.1482×10^{-24} esu, β ; 1 a.u. = 8.6393×10^{-33} esu). The mean polarizability (α), anisotropy of polarizability ($\Delta\alpha$) and the average value of the first hyperpolarizability (β) are calculated. The calculated parameters determined above and electronic dipole moment $\{\mu_i (i = x, y, z)\}$ and total dipole moment μ_{tot} for 3,4-DFA molecule are given in Table S3.

The higher values of dipole moment, molecular polarizability, and hyperpolarizability are important and well known for more active NLO properties. The headline molecule has relatively homogeneous charge distribution and it does not have large dipole moment. The dipole moment was computed as 4.2458 Debye (D). The polarizability and anisotropy of the polarizability of the title molecule is calculated $11.524614 \times 10^{-24}$ and $27.32059234 \times 10^{-24}$ esu, respectively. The magnitude of the molecular hyperpolarizability β , is one of the important key factors in a NLO system. The first hyperpolarizability value (β) of 3,4-DFA molecule is also computed to $1651.535286 \times 10^{-33}$ esu. The first hyperpolarizability, polarizability, anisotropy of the polarizability and dipole moment values of 3,4-DFA are larger than those of urea, compared the common values of based compound.

Reduced density gradient – RDG

Johnson and co-workers [86] published an approach to investigate a weak interactions in real space based on the electron density

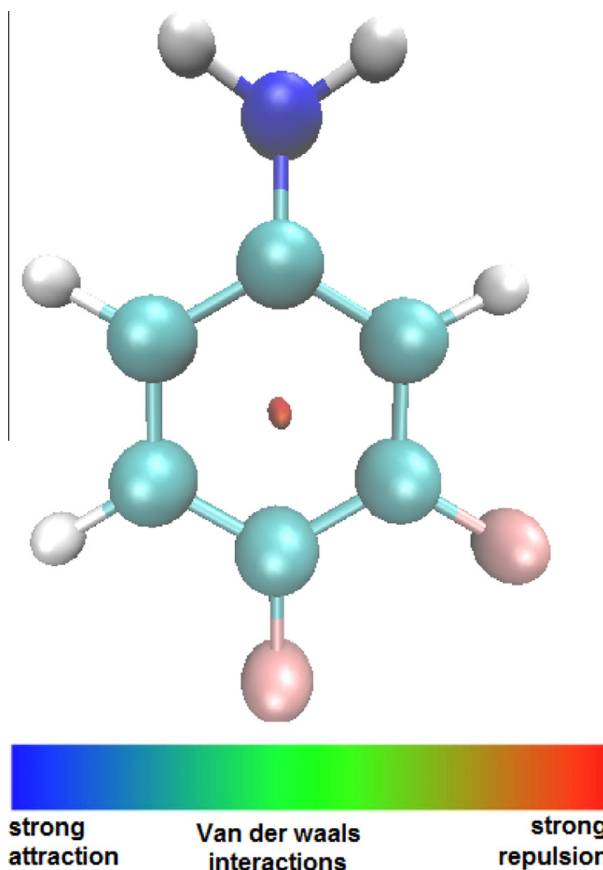


Fig. 12. The surfaces are colored on a blue–green–red scale according to values of $\text{sign } \lambda_2$. (For interpretation of the references to color in this figure legend, the reader is referred to the web version of this article.)

and its derivatives called RDG is dimensionless quantity defined as, following:

$$\text{RDG}(r) = \frac{1}{2(3\pi^2)^{1/3}} \frac{|\nabla\rho(r)|}{\rho(r)^{4/3}}$$

The region with low electron density and low RDG value obtained density and its first derivative, indicate weak interactions. To learn about the interaction in more detail, the sign of λ_2 is used to distinguish the bonded ($\lambda_2 < 0$) from non-bonded ($\lambda_2 > 0$) interactions. The sign of λ_2 multiplied electron density ρ obtained the plots of RDG versus permit to investigate and visualize of a wide range of interactions types. The RDG calculations are performed by Multiwfn [87] and plotted by VMD program [88], respectively. The RDG versus sign (λ_2) ρ (electron density value) peaks provide information about the strength of interaction. There is one spike in the low-density, low gradient region as seen in Fig. 11, indicative of strong repulsion positive values of sign (λ_2) ρ . The RDG = 0.1 lines cross repulsion spikes.

Large, positive values of sign (λ_2) ρ are indicated that strong repulsion interactions and negative ones stronger attractive interactions. The strength of weak interactions have positive correlations with electron density ρ in corresponding region, Van der Waals interaction regions always have very small ρ , while the regions correspond to strong steric effect and hydrogen bond always have relative large ρ . The regions are identified by color as different type seen from Fig. 12. The color from blue to red means from stronger attraction to repulsion, respectively. The center of rings for 3,4-DFA molecule show that strong steric effect, filled by red color. The RDG of molecule are contributed in literature.

Conclusions

This paper we investigated both theoretical and experimental spectroscopic study performed on FT-IR, FT-Raman, NMR and UV spectra of 3,4-DFA molecule. To have more information on the structural parameters, the optimized geometric parameters were determined theoretically at B3LYP/6-311++G(d,p) level of theory and compared of the X-ray results of base and similar molecular architecture of aniline. The vibrational characteristics of the title molecule were recorded by experimental and theoretical quantum chemical methods and their PED. The fundamental modes are also compared with the related molecules based on most important regions. The NMR spectra (^1H and ^{13}C NMR) of 3,4-DFA molecule were saved tentative and theoretical. They were compared after than showed a very good agreement both for ^1H and ^{13}C NMR. The UV-Vis spectral analyses of the molecule were also investigated for gas phase, in ethanol and water solvents. Moreover, the frontier molecular orbitals, density of states (TDOS, PDOS and COOP or OPDOS), MEPs contour/surface of the molecule were also prepared. The statistical thermodynamics properties were also obtained according to variation temperature. It is seen that statistical thermodynamics properties increase with the increasing temperature. Eventually the whole shebang of the predicted parameters was indicated that well concordance and acceptable agreement.

Acknowledgement

This work was supported by the Celal Bayar University Research Fund through research Grant No.: FBE-2011/70.

Appendix A. Supplementary data

Supplementary data associated with this article can be found, in the online version, at <http://dx.doi.org/10.1016/j.saa.2015.01.079>.

References

- [1] J. Whysner, L. Verna, G.M. Williams, *Pharmacol. Ther.* 71 (1996) 107–126.
- [2] P. Kearney, D. Kaufman, *Herbicides: Chemistry, Degradation and Mode of Action*, Marcel Dekker Inc., 1975.
- [3] S. Gheewala, A. Annachhatre, *Water Sci. Technol.* 36 (1997) 53–63.
- [4] S. Lacorte, M.-C. Perrot, D. Fraisse, D. Barceló, *J. Chromatogr. A* 833 (1999) 181–194.
- [5] A. Heaton, M. Hill, F. Drakesmith, *J. Fluor. Chem.* 81 (1997) 133–138.
- [6] H. Cerecetto, W. Porcal, *Mini Rev. Med. Chem.* 5 (2005) 57–71.
- [7] I. Sánchez, M.D. Pujol, *Tetrahedron* 55 (1999) 5593–5598.
- [8] A.L. Sharma, S. Annapoorni, B.D. Malhotra, *Curr. Appl. Phys.* 3 (2003) 239–245.
- [9] J. Niessen, U. Schröder, M. Rosenbaum, F. Scholz, *Electrochem. Commun.* 6 (2004) 571–575.
- [10] J.C. Evans, *Spectrochim. Acta* 16 (1960) 428–442.
- [11] G. Roussy, A. Nonat, *J. Mol. Spectrosc.* 118 (1986) 180–188.
- [12] D.G. Lister, J.K. Tyler, J.H. Hög, N.W. Larsen, *J. Mol. Struct.* 23 (1974) 253–264.
- [13] G. Schultz, G. Portalone, F. Ramondo, A. Domenicano, I. Hargittai, *Struct. Chem.* 7 (1996) 59–71.
- [14] M. Fukuyo, K. Hirotsu, T. Higuchi, *Acta Crystallogr. B* 41 (1982) 640–643.
- [15] M. Castellà-Ventura, E. Kassab, *Spectrochim. Acta A* 50 (1994) 69–86.
- [16] A.-D. Gorse, M. Pesquer, *J. Mol. Struct. Theochem* 281 (1993) 21–32.
- [17] C. Bock, P. George, M. Trachtman, *Theor. Chem. Acc. Theory, Comput. Model. (Theor. Chim. Acta)* 69 (1986) 235–245.
- [18] Y. Wang, S. Saebo, C.U. Pittman, *J. Mol. Struct. Theochem* 281 (1993) 91–98.
- [19] E. Akalin, S. Akyüz, *J. Mol. Struct.* 482–483 (1999) 175–181.
- [20] M.E. Vaschetto, B.A. Retamal, A.P. Monkman, *J. Mol. Struct. Theochem* 468 (1999) 209–221.
- [21] J.C. Jiang, C.E. Lin, *J. Mol. Struct. Theochem* 392 (1997) 181–191.
- [22] M. Alcolea Palafox, J.J. Núñez, M. Gil, M.A. Palafox, *J. Mol. Struct. Theochem* 593 (2002) 101–131.
- [23] I. López-Tocón, M. Becucci, G. Pietraperzia, E. Castellucci, J. Otero, *J. Mol. Struct.* 565–566 (2001) 421–425.
- [24] N.W. Larsen, E.L. Hansen, F.M. Nicolaisen, *Chem. Phys. Lett.* 43 (1976) 584–586.
- [25] R.A. Kydd, P.J. Krueger, *Chem. Phys. Lett.* 49 (1977) 539–543.
- [26] M.A. Shashidhar, K.S. Rao, E.S. Jayadevappa, *Spectrochim. Acta A* 26 (1970) 2373–2377.
- [27] R.A. Kydd, P.J. Krueger, *J. Chem. Phys.* 69 (1978) 827–832.
- [28] M. Honda, A. Fujii, E. Fujimaki, T. Ebata, N. Mikami, *J. Phys. Chem. A* 107 (2003) 3678–3686.
- [29] B.B. Lal, G.D. Brauh, I.S. Singh, *Curr. Sci.* 40 (1971) 655–656.
- [30] V. Mukherjee, K. Singh, N.P. Singh, R.A. Yadav, *Spectrochim. Acta A* 73 (2009) 44–53.
- [31] V. Mukherjee, N.P. Singh, R.A. Yadav, *Spectrochim. Acta A* 73 (2009) 249–256.
- [32] S.K. Pathak, R. Srivastava, A.K. Sachan, O. Prasad, L. Sinha, A.M. Asiri, M. Karabacak, *Spectrochim. Acta A* 135 (2015) 283–295.
- [33] P.M. Wojciechowski, D. Michalska, *Spectrochim. Acta A* 68 (2007) 948–955.
- [34] M. Govindarajan, M. Karabacak, S. Periandy, D. Tanuja, *Spectrochim. Acta A* 97 (2012) 231–245.
- [35] A.D. Becke, *J. Chem. Phys.* 98 (1993) 5648–5652.
- [36] A.D. Becke, *Phys. Rev. A* 38 (1988) 3098–3100.
- [37] C. Lee, W. Yang, R.G. Parr, *Phys. Rev. B* 37 (1988) 785–789.
- [38] M.J. Frisch et al., *Gaussian Inc., Wallingford, CT*, 2009.
- [39] N. Sundaraganesan, S. Ilakiamani, H. Saleem, P.M. Wojciechowski, D. Michalska, *Spectrochim. Acta A* 61 (2005) 2995–3001.
- [40] M. Karabacak, M. Kurt, M. Cinar, A. Coruh, *Mol. Phys.* 107 (2009) 253–264.
- [41] J.B. Foresman, A. Frisch, *Gaussian Inc, Pittsburgh, PA*, 1996, pp. 98–99.
- [42] M.H. Jamróz, *Spectrochim. Acta A* 114 (2013) 220–230.
- [43] R. Dennington, T. Keith, J. Millam, *GaussView, Version 5*, 2009.
- [44] R. Ditchfield, *J. Chem. Phys.* 56 (1972) 5688–5691.
- [45] K. Wolinski, J.F. Hinton, P. Pulay, *J. Am. Chem. Soc.* 112 (1990) 8251–8260.
- [46] N.M. O'Boyle, A.L. Tenderholt, K.M. Langner, *J. Comput. Chem.* 29 (2008) 839–845.
- [47] M. Karabacak, D. Karagöz, M. Kurt, *J. Mol. Struct.* 892 (2008) 25–31.
- [48] M. Karabacak, D. Karagöz, M. Kurt, *Spectrochim. Acta A* 72 (2009) 1076–1083.
- [49] D. Christen, D. Damiani, D.G. Lister, *J. Mol. Struct.* 41 (1977) 315–317.
- [50] R.A. Kydd, S. Mah, *Spectrochim. Acta A* 38 (1982) 1031–1034.
- [51] I. Altarawneh, K. Altarawneh, A.H. Al-Muhtaseb, S. Alrawadieh, M. Altarawneh, *Comput. Theor. Chem.* 985 (2012) 30–35.
- [52] T. Karthick, V. Balachandran, S. Perumal, A. Nataraj, *Spectrochim. Acta A* 107 (2013) 72–81.
- [53] P. Wojciechowski, K. Helios, D. Michalska, *Vib. Spectrosc.* 57 (2011) 126–134.
- [54] L. Nygaard, I. Bojesen, T. Pedersen, J. Rastrup-Andersen, *J. Mol. Struct.* 2 (1968) 209–215.
- [55] M. Colapietro, A. Domenicano, C. Marcianti, G. Portalone, *Acta Crystallogr. B Struct. Sci.* 37 (1981) 387–394.
- [56] A. Altun, K. Gölcük, M. Kumru, *J. Mol. Struct. Theochem* 637 (2003) 155–169.
- [57] T. Sivarajini, S. Periandy, M. Govindarajan, M. Karabacak, A.M. Asiri, *J. Mol. Struct.* 1056–1057 (2014) 176–188.
- [58] S. Ramalingam, S. Periandy, B. Narayanan, S. Mohan, *Spectrochim. Acta A* 76 (2010) 84–92.
- [59] R.M. Silverstein, G.C. Bassler, T.C. Morrill, *Spectrometric Identification of Organic Compounds*, Wiley, 1981.
- [60] M. Arivazhagan, D. Anitha Rexalin, *Spectrochim. Acta A* 96 (2012) 668–676.
- [61] N. Sundaraganesan, J. Karpagam, S. Sebastian, J.P. Cornard, *Spectrochim. Acta A* 73 (2009) 11–19.
- [62] V. Rastogi, M.A. Palafox, R.P. Tanwar, L. Mittal, *Spectrochim. Acta A* 58 (2002) 1987–2004.

- [63] C.S. Hiremath, T. Sundius, *Spectrochim. Acta Part A Mol. Biomol. Spectrosc.* 74 (2009) 1260–1267.
- [64] S. Singh, N. Singh, *Indian J. Pure Appl. Phys.* 7 (1969) 250–252.
- [65] P. Wojciechowski, *J. Fluor. Chem.* 154 (2013) 7–15.
- [66] S.K. Tiwari, K.N. Upadhyay, *Indian J. Pure Appl. Phys.* 6 (1968) 698.
- [67] M. Karabacak, E. Kose, A. Atac, M. Ali Cipiloglu, M. Kurt, *Spectrochim. Acta A* 97 (2012) 892–908.
- [68] M. Karabacak, E. Kose, M. Kurt, *J. Raman Spectrosc.* 41 (2010) 1085–1097.
- [69] R.M. Silverstein, F.X. Webster, D.J. Kiemle, *Spectrometric Identification of Organic Compounds*, John Wiley & Sons, 2005.
- [70] H.M. Badawi, W. Förner, S.A. Ali, *Spectrochim. Acta A* 112 (2013) 388–396.
- [71] G. Varsányi, *Assignments for Vibrational Spectra of Seven Hundred Benzene Derivatives*, Halsted Press, 1974.
- [72] T. Schlick, *Molecular Modeling and Simulation: An Interdisciplinary Guide: An Interdisciplinary Guide*, second ed., Springer, New York, USA, 2010.
- [73] N. Subramanian, N. Sundaraganesan, J. Jayabharathi, *Spectrochim. Acta A* 76 (2010) 259–269.
- [74] H.O. Kalinowski, S. Berger, S. Braun, *Carbon-13 NMR Spectroscopy*, 1988.
- [75] K. Pihlaja, E. Kleinpeter, *Carbon-13 NMR Chemical Shifts in Structural and Stereochemical Analysis*, VCH, 1994.
- [76] A.U. Rani, N. Sundaraganesan, M. Kurt, M. Cinar, M. Karabacak, *Spectrochim. Acta Part A Mol. Biomol. Spectrosc.* 75 (2010) 1523–1529.
- [77] D. Guillaumont, S. Nakamura, *Dyes Pigm.* 46 (2000) 85–92.
- [78] J. Fabian, *Dyes Pigm.* 84 (2010) 36–53.
- [79] R.G. Parr, P.K. Chattaraj, *J. Am. Chem. Soc.* 113 (1991) 1854–1855.
- [80] R. Hoffman, *Solids and Surfaces: A Chemist's View of Bonding in Extended Structures*, 1988.
- [81] T. Hughbanks, R. Hoffmann, *J. Am. Chem. Soc.* 105 (1983) 3528–3537.
- [82] J.G. Malecki, *Polyhedron* 29 (2010) 1973–1979.
- [83] M. Chen, U.V. Waghmare, C.M. Friend, E. Kaxiras, *J. Chem. Phys.* 109 (1998) 6854–6860.
- [84] N. Okulik, A.H. Jubert, *Internet Electron. J. Mol. Des.* 4 (2005) 17–30.
- [85] F.J. Luque, J.M. López, M. Orozco, *Theor. Chem. Acc. Theory, Comput. Model. (Theor. Chim. Acta)* 103 (2000) 343–345.
- [86] E.R. Johnson, S. Keinan, P. Mori-Sánchez, J. Contreras-García, A.J. Cohen, W. Yang, *J. Am. Chem. Soc.* 132 (2010) 6498–6506.
- [87] T. Lu, F. Chen, *J. Comput. Chem.* 33 (2012) 580–592.
- [88] W. Humphrey, A. Dalke, K. Schulten, *J. Mol. Graph.* 14 (1996) 33–38.